AIP | Journal of Applied Physics

Phase-field simulation of phase coarsening at ultrahigh volume fractions

K. G. Wang, X. Ding, Kunok Chang, and L. Q. Chen

Citation: J. Appl. Phys. **107**, 061801 (2010); doi: 10.1063/1.3340517
View online: http://dx.doi.org/10.1063/1.3340517
View Table of Contents: http://jap.aip.org/resource/1/JAPIAU/v107/i6
Published by the American Institute of Physics.

Phase-field simulation of phase coarsening at ultrahigh volume fractions

K. G. Wang,[1,a)] X. Ding,[1] Kunok Chang,[2] and L. Q. Chen[2]
[1]*Department of Physics and Space Science, Materials Science and Nanotechnology Institute, Florida Institute of Technology, Melbourne, Florida 32901-6975, USA*
[2]*Department of Materials Science and Engineering, The Pennsylvania State University, University Park, Pennsylvania 16802, USA*

(Received 30 December 2008; accepted 14 July 2009; published online 26 March 2010)

In this paper, the dynamics of phase coarsening at ultrahigh volume fractions ($0.9 \leq V_V \leq 0.96$) is first studied based on two-dimensional phase-field simulations by numerically solving the time-dependent Ginzburg–Landau and Cahn–Hilliard equations. It is shown that the cubic average radius of particles is approximately proportional to time that is in good agreement with one of experimental observations. The microstructural evolutions for different ultrahigh volume fractions are shown. The scaled particle size distribution as functions of the dispersoid volume fraction is presented. The interesting finding is that the particle size distribution derived from our simulations at ultrahigh volume fractions is close to Wagner's particle size distribution due to interface-controlled ripening rather than Hillert's grain size distribution in grain growth. The changes of shapes of particles are carefully studied with increase in volume fraction. It is found that some liquid-filled triple junctions are formed as a result of particle shape accommodation at ultrahigh volume fraction, $V_V \approx 0.96$. © *2010 American Institute of Physics*.
[doi:10.1063/1.3340517]

I. INTRODUCTION

Phase coarsening is a common relaxation process during late-stage microstructural evolution that leads to a decrease in the excess total interfacial energy of two-phase systems. During phase coarsening, larger particles tend to grow by absorbing solute atoms at the expense of small particles that tend to dissolve by losing them. Over time, this "competitive diffusion" results in an increase in the average size of the particle population, and in a concomitant decrease in the number density of particles. The study of phase-coarsening kinetics during microstructural evolution is critical to a variety of industrial applications involving two-phase systems in which the dispersed phase controls the properties of the material. Liquid-phase sintering, casting, and spray deposition are just a few examples of processes in which the coarsening process has important technological implications. There have been numerous experimental, theoretical, and computational attempts over the last decades to understand the kinetics of phase coarsening. The first successful theory for diffusion-controlled phase coarsening was proposed in 1961 by Lifshitz and Slyozov[1] and Wagner.[2] The predictions of this model—now referred to as the LSW theory—are strictly valid only in the case of vanishing volume fractions ($V_V \rightarrow 0$), entailing a growth law of the form

$$\langle R(t)\rangle^n - \langle R(t_0)\rangle^n = K_n(t - t_0), \tag{1}$$

where $\langle R(t)\rangle$, $\langle R(t_0)\rangle$, and K_n denote, respectively, the average particle radius at time t, the average radius at initial time t_0, and a proportionality constant. n is called scaling exponent, and $1/n$ is called time exponent. For diffusion-controlled coarsening, the scaling and time exponents take on the values of 3 and 1/3, respectively; on the other hand, for normal grain growth, $n=2$.[3,4]

Although progress has been made in the thermodynamics and kinetics of phase coarsening over the past two decades, there remains a significant challenge to fundamentally understand the coarsening kinetics at ultrahigh volume fractions (ca. $V_V \geq 0.9$). Recently, Wang *et al.*[5,6] reviewed the status of theoretical, computational, and experimental studies of phase coarsening, following two earlier reviews.[7,8] In order to take into account the effects of nonzero volume fraction, a number of mean-field theories of coarsening have been developed over the past 40 years.[9–15] However, all of them are strictly valid only at low volume fractions (<0.1).[16] However, Wang *et al.*[21,22] developed diffusion screening theory, which is valid for the range of $0 < V_V < 0.33$. Marsh and Glicksman[17] introduced the concept of a statistical "field cell" acting around each size class of the particles undergoing phase coarsening, and obtained normalized coarsening rates that are in good agreement with data derived from various liquid-phase sintering experiments, particularly in the range $0.3 \leq V_V \leq 0.6$. Therefore, there is no existing theory for coarsening in the ultrahigh volume fraction regime.

The earliest attempt to employ computer simulations for particle coarsening was published in 1973 by Weins and Cahn.[18] They employed several particles in various spatial configurations to demonstrate the basic coarsening interactions during sintering. Their study was followed by the publication of multiparticle simulations by Voorhees and Glicksman,[19] who systematically studied microstructural evolution using several hundred randomly distributed particles. Later, Beenaker[20] improved multiparticle simulation procedures and was able to increase the total number of particles to several thousands. More recently, a further development by Wang *et al.* resulted in additional improvement in

a)Electronic mail: kwang@fit.edu.

the accuracy of simulating three-dimensional (3D) phase coarsening by multiparticle diffusion method.[21–28] The multiparticle diffusion simulations were carried out in the range of $10^{-10} \leq V_V \leq 0.55$. More recently, the phase-field method has been employed to model the microstructural coarsening process. Chen *et al.* performed two-dimensional (2D) phase-field simulations for volume fractions up to $V_V=0.9$.[29] However, phase coarsening in the ultrahigh volume fraction regime ($0.9 \leq V_V < 1$) remains to be explored.

There are several advanced experimental methods developed to study and quantify the phenomenon of late-stage phase coarsening. Baldan[30] reviewed the status of experimental studies to quantify phase coarsening in nickel-base superalloys, especially those based on the binary system Ni–Al. Most experimental studies fall in the volume fraction range $0 < V_V < 0.5$ and have been based on 2D microstructures. Hardy and Voorhees[31] experimentally examined phase coarsening in the volume fraction range from 0.6 to 0.9 in Pb–Sn alloys and observed cube-root kinetics. Sok and Yoon[32] experimentally studied the kinetics in Fe–Cu and Co–Cu alloys for the volume fraction range from 0.34 to 0.95 and observed cube-root time kinetics. However, Kailasam *et al.* experimentally investigated the kinetics in Sn–Pb alloys for the volume fraction range from 0.5 to 0.95.[33] They found that when the volume fraction becomes ultrahigh ($V_V=0.90$), instead of cube-root of time kinetics, the fourth root of time kinetics was observed. They also found that, as the volume fraction drops from $V_V=0.90$, the temporal exponent lies between 1/4 and 1/3, depending on the volume fraction. These findings are contrary to all other experimental results reported for this range of volume fractions. There is no other confirmation for these findings. On the other hand, it is well known that when $V_V=1$ the phase coarsening corresponds to grain growth, and the kinetics are square root. However, no definitive conclusions could be reached regarding how $1/n$ changes with V_V—i.e., does the time exponent manifest a crossover from 1/3 to 1/2 somewhere at ultrahigh volume fractions of the coarsening phase?

The main objective of this paper is to study the crossover behaviors for some physical quantities such as the time or scaling exponents and particle size distribution (PSD) in the range of ultrahigh volume fractions ($0.9 \leq V_V \leq 0.96$) where analytical theories are the most difficult to be developed using 2D phase-field simulations. Using the phase-field simulations we will obtain the detailed temporal microstructural evolution for the phase coarsening. We will systematically study the effects of volume fraction on the average size of particle, the scaling exponent n, and PSD in the unexplored regime of ultrahigh volume fractions. The organization of this paper is as follows. In Sec. II, we briefly describe phase-field model for phase coarsening. In Sec. III, we provide details of phase field simulation. In Sec. IV, we present the results from our phase-field simulation and discussion. Finally, in Sec. V, we conclude with a summary.

II. PHASE-FIELD MODEL FOR PHASE COARSENING

One of the main advantages of the phase-field approach is its ability to handle complex microstructures in the ultrahigh volume fraction regime. It has been applied to different material processes, including solidifications[34] and Boettinger *et al.*,[35] solid state phase transformations,[36] and grain growth.[37–40] The simulating microstructure consists of particles of one phase dispersed in the continuous matrix of another phase. In this microstructure, the solubilities or equilibrium compositions are c_α and c_β for the matrix phase and second phase, respectively. A two-phase microstructure in a binary system is described by a composition field variable $c(\vec{\mathbf{r}})$, which represents the spatial compositional distribution in space, and orientation field variables that represent grains/particles of a given crystallographic orientation in space, $\eta_i(\vec{\mathbf{r}}), (i=1,2,\ldots,p)$. In the following, particle and grain can be interchangeable. These variables change continuously in space and assume values ranging from -1.0 to 1.0. All orientation field variables are zero in the matrix phase, simulating a liquid or disordered phase. $c(\vec{\mathbf{r}})$ takes the value of c_α within the matrix phase and c_β within a second phase grain. $c(\vec{\mathbf{r}})$ has intermediate values between c_α and c_β at the interfacial region between the matrix phase and a second-phase grain. The total energy of the inhomogeneous system is written as

$$F(c,\eta_i) = \int_\Omega \left[f_0(c,\eta_i) + \frac{1}{2}\kappa_c(\nabla c)^2 + \sum_{i=1}^{p} \frac{1}{2}\kappa_i(\nabla \eta_i)^2 \right] dv, \tag{2}$$

where Ω represents the domain of the binary system. ∇c and $\nabla \eta_i$ are gradients of composition and orientation fields, κ_c and κ_i are the gradient energy coefficients, and f_0 is the local free energy density, which is assumed to be[29]

$$f_0 = f_1(c) + \sum_{i=1}^{p} f_2(c,\eta_i) + \sum_{i=1}^{p}\sum_{j\neq i}^{p} f_3(\eta_i,\eta_j), \tag{3}$$

where

$$f_1(c) = -\frac{A}{2}(c-c_m)^2 + \frac{B}{4}(c-c_m)^4 + \frac{E_\alpha}{4}(c-c_\alpha)^4 + \frac{E_\beta}{4}(c-c_\beta)^4,$$

$$f_2(c,\eta_i) = -\frac{\gamma}{2}(c-c_\alpha)^2\eta_i^2 + \frac{\delta}{4}\eta_i^4,$$

$$f_3(\eta_i,\eta_j) = \frac{\epsilon_{ij}}{2}\eta_i^2\eta_j^2, \tag{4}$$

where $c_m=(c_\alpha+c_\beta)/2$, and A, B, E_α, E_β, γ, δ, and ϵ_{ij} are phenomenological parameters. These parameters are chosen in such a way that f_0 has 2p degenerate minima with equal depth located at $(\eta_1,\eta_2,\ldots,\eta_p) = (1,0,\ldots,0),(0,1,\ldots,0),\ldots,(0,0,\ldots,1)$ at the equilibrium concentration c_β. This requirement ensures that each point in space belongs to a grain with a given orientation of a given phase.

This formulation guarantees that, when two particles with different orientations are in contact with each other, a grain boundary forms. Two particles will coalesce when they have the same orientation. In our study, we focus on the

coarsening stage. The driving force for particle coarsening is minimization of total surface energy (grain boundary energy and interfacial energy). Therefore, as long as the correct grain boundary and interfacial energies are obtained, the exact form of the free energy density f_0 is not an issue. Free energy density f_0 determines the driving force for the phase transformation, i.e., for the nucleation and growth stages.

The temporal evolution of the field variables is obtained by solving the Cahn– Hilliard and time-dependent Ginzburg–Landau equations,[41,42]

$$\frac{\partial c(\vec{\mathbf{r}},t)}{\partial t} = \nabla\left\{ D\,\nabla\left[\frac{\delta F}{\delta c(\vec{\mathbf{r}},t)}\right]\right\}, \tag{5}$$

and

$$\frac{\partial \eta_i(\vec{\mathbf{r}},t)}{\partial t} = -L_i\frac{\delta F}{\delta \eta_i(\vec{\mathbf{r}},t)}; \quad i=1,\ldots p, \tag{6}$$

where L_i and D are kinetic coefficients related to grain boundary mobilities and the atomic diffusion coefficient. The difference between the kinetic equations for the orientation field variables $\eta_i(\vec{\mathbf{r}})$ and the composition field $c(\vec{\mathbf{r}})$ comes from the fact that $c(\vec{\mathbf{r}})$ is conserved field, due to the requirement of mass conservation, and the orientation fields are nonconserved variables.

The energy of a planar grain boundary, σ_{gb}, between a grain of orientation i and another grain of orientation j for two second-phase grains can be written as

$$\sigma_{gb} = \int_{-\infty}^{+\infty}\left[\Delta f(\eta_i,\eta_j,c) + \frac{\kappa_c}{2}\left(\frac{dc}{dx}\right)^2 + \frac{\kappa_i}{2}\left(\frac{d\eta_i}{dx}\right)^2 + \frac{\kappa_j}{2}\left(\frac{d\eta_j}{dx}\right)^2\right]dx, \tag{7}$$

in which

$$\Delta f(\eta_i,\eta_j,c) = f_0(\eta_i,\eta_j,c) - f_0(\eta_{i,e},\eta_{j,e},c_\beta) - (c-c_\beta)\times\left(\frac{\partial f_0}{\partial c}\right)_{\eta_{i,e},\eta_{j,e},c_\beta}, \tag{8}$$

where $f_0(\eta_{i,e},\eta_{j,e},c_\beta)$ represents the free energy density minimized with respect to η_i and η_j at the equilibrium composition of the second phase c_β. Similarly, the interphase boundary energy between the matrix phase and a second phase grain with orientation i, σ_{in}, can be defined through elimination of η_j in Eqs. (7) and (8).

III. SIMULATION DETAILS

The phenomenological parameters $c_m=(c_\alpha+c_\beta)/2$, and A, B, E_α, E_β, γ, δ, and ϵ_{ij} are chosen in such a way that f_0 has 2p degenerate minima with equal depth located at $(\eta_1,\eta_2,\ldots,\eta_p)=(1,0,\ldots,0),(0,1,\ldots,0),\ldots,(0,0,\ldots,1)$ at the equilibrium concentration c_β. In fact, the condition of minima of free energy can first determine the relationship between γ and δ. The condition of minima of free energy is given by

$$\left.\frac{\partial f_0}{\partial \eta_i}\right|_{\eta_i=1,\eta_{j\neq i}=0,c=c_\beta} = 0. \tag{9}$$

Substituting the free energy in Eq. (2) into Eq. (9) and doing some mathematical calculation, we have

$$\gamma = \frac{\delta}{(c_\alpha - c_\beta)^2}. \tag{10}$$

This relationship between γ and δ is general and is applied in our simulations.

To numerically solve the Cahn–Hilliard and time-dependent Ginzburg–Landau equations, the following discretization of the Laplacian with respect to space is employed:

$$\nabla^2 g_i = \frac{1}{(\Delta x)^2}\left[\frac{1}{2}\sum_{j=1}^{N_f}(g_j-g_i) + \frac{1}{4}\sum_{j'=1}^{N_s}(g_{j'}-g_i)\right], \tag{11}$$

where g is any function, Δx denotes the grid size, and j and j' run over from 1 to the number of the first nearest neighbors of i, N_f, and the number of the second nearest neighbors of i, N_s, in the grid, respectively. For the time evolution of fields, we use the following Euler forward scheme:

$$\phi(t+\Delta t) = \phi(t) + \frac{d\phi}{dt}\Delta t, \tag{12}$$

where ϕ and Δt are any function and the time step for integration in time, respectively. To avoid boundary effects in the simulations periodic boundary conditions are applied in all simulations.

In this paper, we will employ phase field model to simulate 2D phase coarsening for the ultrahigh volume fraction regime. We will perform systematic simulations at different volume fractions within the volume fraction regime $0.9 \leq V_V \leq 0.96$ to extract the coarsening kinetics as well as the temporal evolution of statistical information about the microstructures. The kinetic coefficients D and L_i in Eqs. (5) and (6) are assumed to be 1 in the simulations. Therefore, it is assumed that both diffusivities and mobilities in both phases are the same. The phenomenological parameters are chosen as $c_\alpha=0.05$, $c_\beta=0.95$, $c_m=(c_\alpha+c_\beta)/2=0.5$, $A=1$, $B=A/(c_\beta-c_\alpha)^2=4.94$, $\delta=1.0$, $\gamma=\delta/(c_\beta-c_\alpha)^2=1.23$, $E_\alpha=E_\beta=1.23$, and $\epsilon_{ij}=3.0$. The gradient coefficients k_i, k_j, and k_c are assumed to be 3.0. These chosen parameters deliver an energetic ratio $\sigma_{gb}/\sigma_{in}=2.927$, which satisfies the total wetting condition.

The number of orientation field variables is 30. The size of simulation box is 512×512, and the space step for integration, $\Delta x=2.0$, and the time step, $\Delta t=0.22$. The initial configuration is generalized by the following way: (1) assigning all the orientation field variables, $\eta_i=0$, on all the grid points with small random values (±0.001); (2) assigning an average concentration, c_{av}, on all the grid points, which is determined by desired equilibrium volume fraction from the formula $c_{av}=c_\beta V_V+(1-V_V)c_\alpha$, with a small random values (±0.01).

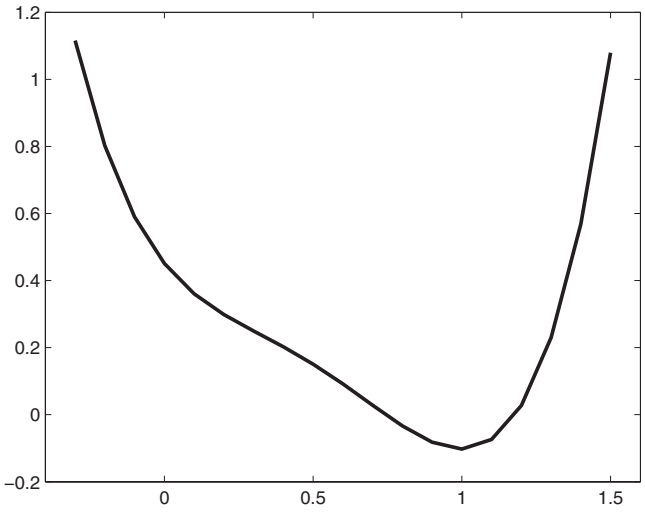

FIG. 1. The first two terms of local free energy density f_0, i.e., $f_1(c)+f_2(c)$, in Eq. (4) vs composition, with considering that total contribution of η_i in both phases to $f_1(c)+f_2(c)$ is 1.

IV. SIMULATION RESULTS AND DISCUSSION

In order to understand how the local free energy density, Eq. (4), changes with the composition, we plot the first two terms of local free energy density f_0, i.e., $f_1(c)+f_2(c)$, in Eq. (4) versus composition in Fig. 1. During the process of plotting Fig. 1 we considered that total contribution of η_i in both phases to $f_1(c)+f_2(c)$ should be 1. Figure 1 shows that the relative minima of the local free energy density without orientation field are located around $c=0.95$ and $c=0.05$.

Figure 2 shows three snapshots of the microstructural evolution for $V_V \approx 0.90$ at the time steps $t=25\,000$, $t=35\,000$, and $t=45\,000$, respectively. The snapshots in Fig. 2 shows that most of small particles surrounding large particles in the snapshot at the time steps $t=25\,000$ are disappeared in the snapshot at longer time steps $t=45\,000$. The shapes of particles at ultrahigh volume fraction are different from circle shapes at the case of lower volume fraction. Most particles have curved edges and rounded corners, and few particles have flattened edges. Figure 3 shows three snapshots of the microstructural evolution for $V_V \approx 0.93$ at the time steps $t=25\,000$, $t=35\,000$, and $t=45\,000$, respectively. From the snapshot at longer time steps $t=45\,000$ in Fig. 3, it is observed that most of large particles have sharply flattened edges, but have rounded corners. Most of small particles have curved or rounded sides. Figure 4 shows three snapshots of the microstructural evolution for $V_V \approx 0.96$ at the time steps $t=25\,000$, $t=35\,000$, and $t=45\,000$, respectively. It is shown in the snapshot at longer time steps $t=45\,000$ in Fig. 4 that most of particles have sharply flattened edges, and except a few small particles have curved sides. Many liquid-filled triple junctions are formed as a result of grain shape accommodation at ultrahigh volume fraction, $V_V \approx 0.96$. This similar phenomenon was also observed in experimental work.[33]

The variations of volume fraction versus simulation time for $V_V \approx 0.90$, $V_V \approx 0.93$, and $V_V \approx 0.96$, respectively, are shown in Fig. 5. It is observed that at early stage, i.e., during the simulation time steps smaller 10 000, the volume fractions increase rapidly. After that time, the volume fractions increase gradually with time (time steps smaller than 40 000), and then gradually approach to corresponding equilibrium values of volume fractions.

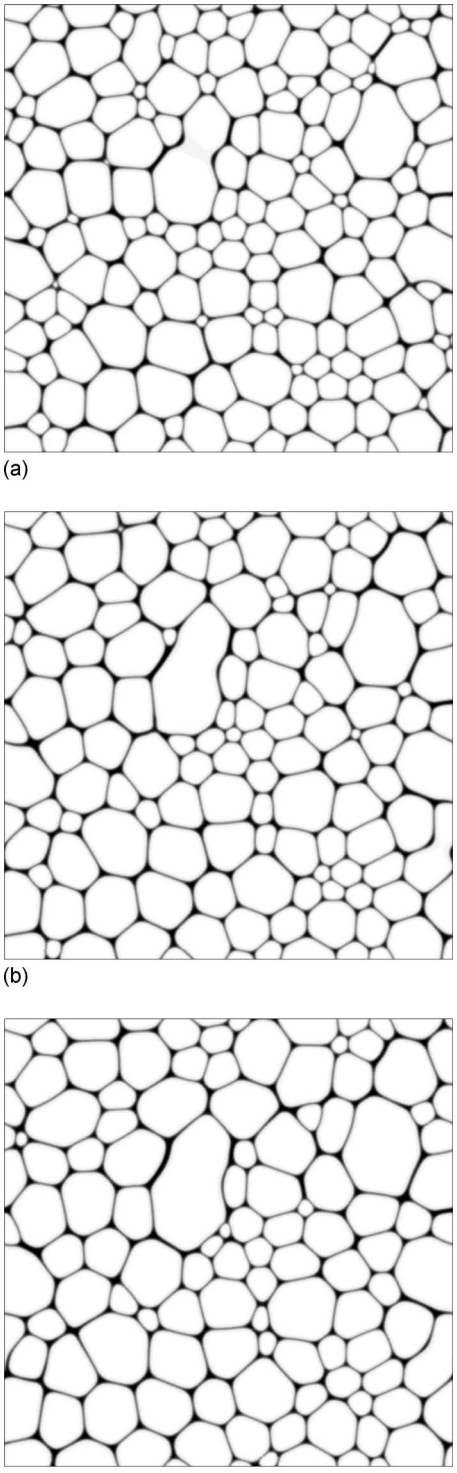

FIG. 2. Microstructural evolution for $V_V \approx 0.90$ and $\kappa_c=2.0$ at the time steps $t=25\,000$, $t=35\,000$, and $t=45\,000$, respectively. The white represents particles of second phase and the black represents liquid phase.

Figure 6 shows the kinetics of phase coarsening, i.e., $\langle R\rangle^3$ versus time for $V_V \approx 0.90$, $V_V \approx 0.93$, and $V_V \approx 0.96$. For $V_V \approx 0.90$, the change of $\langle R\rangle^3$ with time is linear. For $V_V \approx 0.93$ and $V_V \approx 0.96$, the change of $\langle R\rangle^3$ with time can still

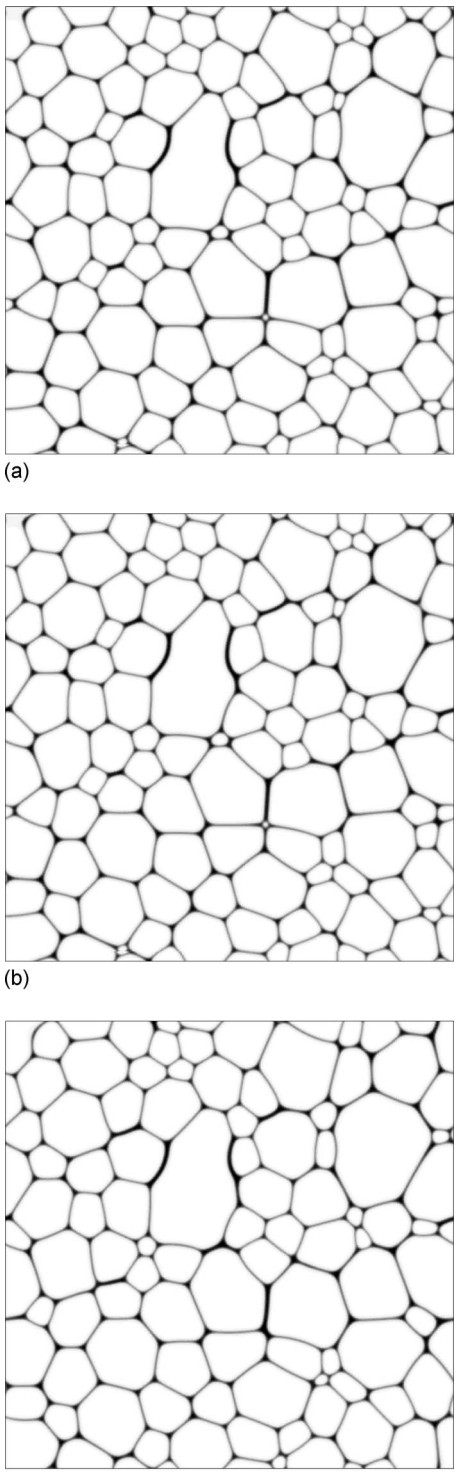

FIG. 3. Microstructural evolution for $V_V \approx 0.93$ at the time steps $t=25\,000$, $t=35\,000$, and $t=45\,000$, respectively. The white represents particles of second phase and the black represents liquid phase.

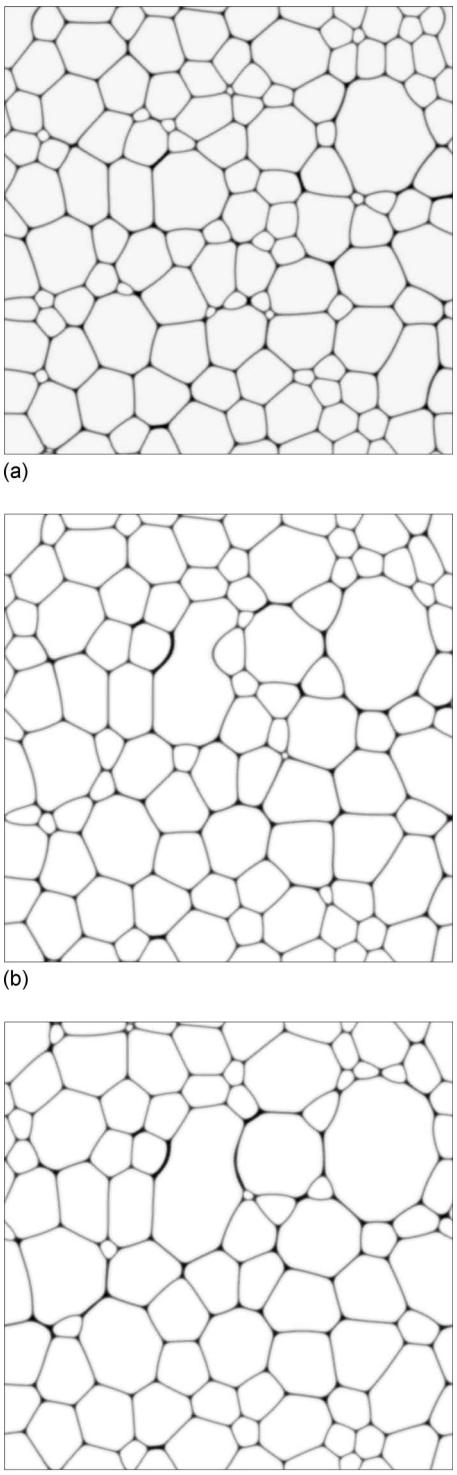

FIG. 4. Microstructural evolution for $V_V \approx 0.96$ at the time steps $t=25\,000$, $t=35\,000$, and $t=45\,000$, respectively. The white represents the particles of second phase and the black represents liquid phase.

fit by approximately linear relation. The relationship that $\langle R\rangle^3$ is proportional to time at volume fractions up to $V_V = 0.95$ was found by Sok and Yoon's experimental work for the system of Co–Cu alloys.[32] However, the experimental work of Kailasam *et al.*[33] showed that $\langle R\rangle^4$ is proportional to time at volume fraction up to $V_V = 0.95$ for the system of Sn–Pb alloys.

Figure 7 shows that the PSD's derived from our simulations for $V_V \approx 0.90$, $V_V \approx 0.93$, and $V_V \approx 0.96$, and Wagner's PSD, Eq. (13). In order to obtain smooth PSD's, three separate simulations with three different seeds of random generators run for each volume fraction. The PSD's in Fig. 7 are averaged over three separate simulation data. The peak of the PSD is lowered down and the width of the PSD increases when volume fraction is increased. This is typical characteristics of phase coarsening. The interesting finding is that the

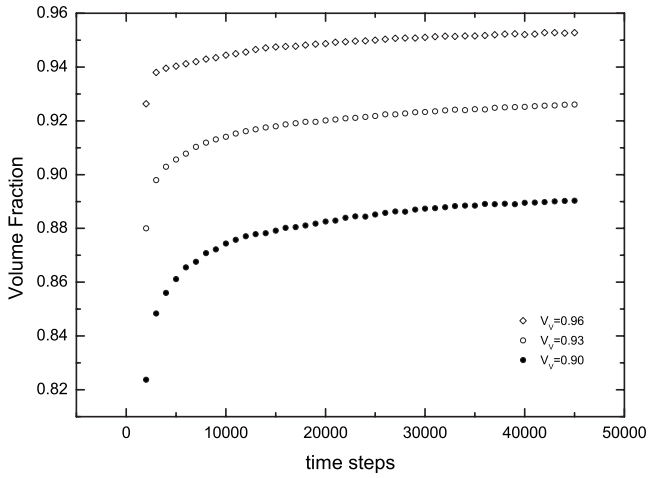

FIG. 5. Variation of volume fractions vs time steps for $V_V \approx 0.90$, $V_V \approx 0.93$, and $V_V \approx 0.96$, respectively. Filled circles, unfilled circles, and unfilled diamonds represent $V_V \approx 0.90$, $V_V \approx 0.93$, and $V_V \approx 0.96$, respectively.

PSD's derived from our simulations at ultrahigh volume fractions is closer to Wagner's PSD. Wagner's PSD (Ref. 2) is for interface-controlled ripening, where some interfacial reaction, rather than volume diffusion through the matrix, becomes rate limiting. Wagner's PSD is written as

$$G(\rho) = \begin{cases} \left[\frac{24\rho}{(2-\rho)^5}\right] \exp\left[\frac{-3\rho}{(2-\rho)}\right], & (\rho < 2) \\ 0 & (\rho \geq 2) \end{cases}. \quad (13)$$

In this paper, we numerically solve both Cahn–Hilliard Eq. (5) and time-dependent Ginzburg–Landau Eq. (6) with consideration of $L_i = D = 1$. However, if D is assumed to be very large relative to L_i, i.e., $L_i \approx 0$, it corresponds to the case of diffusion-controlled phase coarsening. The Eq. (6) is eliminated and only Eq. (5) needs to be numerically solved. Rogers and Desai[43] numerically solved Cahn–Hilliard Eq. (5) and simulated phase coarsening at the cases of lower volume fractions in 1989. This case can be recovered by using the approximation in energetics that $\kappa_c \gg \kappa_i$ and $\kappa_i \approx 0$ in Eq. (2). On the other hand, if L_i is assumed to be very large relative to D, i.e., $D \approx 0$. The Eq. (5) is eliminated and only Eq. (6) needs to be numerically solved. This case corresponds to grain growth. Chen and Yang[38] used this method to simulate 2D grain growth. Krill and Chen[37] extended this method to simulate 3D grain growth. This case can also be recovered by using the approximation in energetics that $\kappa_i \gg \kappa_c$ and $\kappa_c \approx 0$ in Eq. (2).

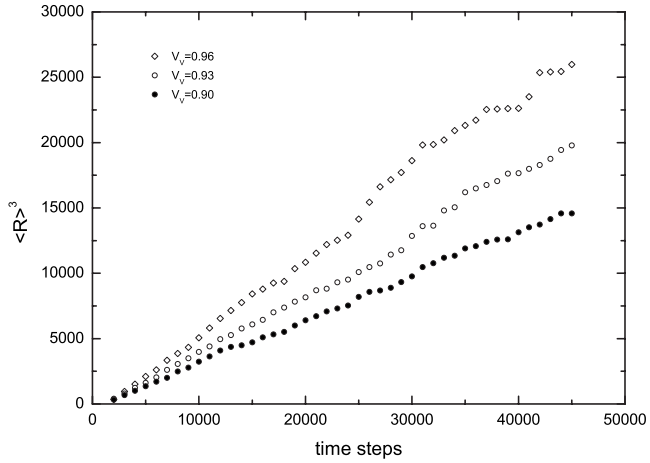

FIG. 6. Variation of $\langle R \rangle^3$ vs time steps for $V_V \approx 0.90$, $V_V \approx 0.93$, and $V_V \approx 0.96$, respectively. Filled circles, unfilled circles, and unfilled diamonds represent $V_V \approx 0.90$, $V_V \approx 0.93$, and $V_V \approx 0.96$, respectively.

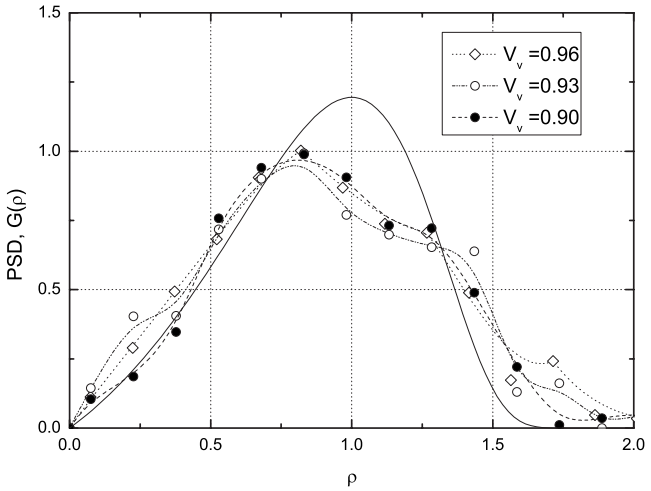

FIG. 7. PSDs, $G(\rho)$, for $V_V \approx 0.90$, $V_V \approx 0.93$, and $V_V \approx 0.96$, where ρ is radius scaled by average radius and Wagner's PSD. Filled circles with dashed line, unfilled circles with dashed line, and unfilled diamonds with dashed line represent $V_V \approx 0.90$, $V_V \approx 0.93$, and $V_V \approx 0.96$, respectively. Solid line represents Wagner's PSD.

In addition, in order to understand the effect of different values of κ_c on the microstructure evolution, we run one simulation at $V_V \approx 0.9$ with $\kappa_c = 2.0$ and other parameters same as the previous simulations. This change results in a tiny change for an energetic ratio $\sigma_{gb}/\sigma_{in} = 2.904$ from 2.927. We compared the microstructures at different times for $\kappa_c = 3.0$ and $\kappa_c = 2.0$ at $V_V \approx 0.9$. What we found is that the microstructures are statistically similar, the kinetics for the two cases are similar, and the PSD's for the two cases are also similar. As an example, Fig. 8 shows that the PSD's for

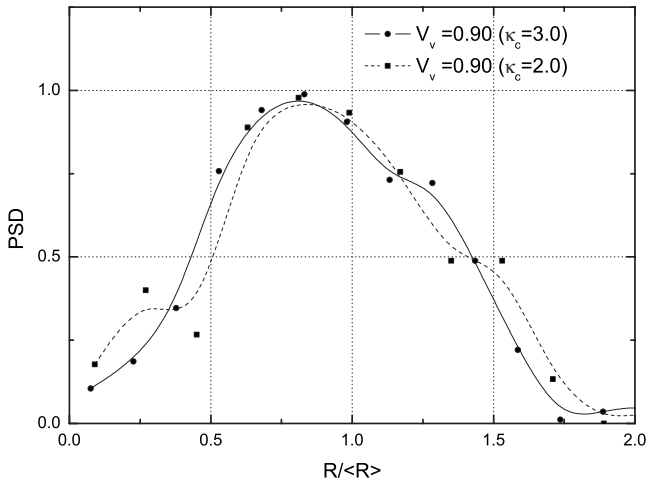

FIG. 8. PSDs, $G(\rho)$, for $V_V \approx 0.90$, but with the parameters $\kappa_c = 2.0$ and $\kappa_c = 3.0$, where ρ is radius scaled by average radius. Filled circles with solid line and filled squares with dashed line represent PSDs for $\kappa_c = 2.0$ and $\kappa_c = 2.0$ at $V_V \approx 0.90$, respectively.

the parameters $\kappa_c=2.0$ and $\kappa_c=3.0$ at $V_V \approx 0.90$. Figure 8 has shown that the two PSD's are statistically the same.

V. CONCLUSIONS

We simulated microstructural evolution in a phase coarsening and kinetics of phase coarsening at ultrahigh volume fractions using phase-field method, i.e., numerically solving the time-dependent Ginzburg–Landau and Cahn–Hilliard equations. We extracted kinetics and PSD's of phase coarsening at ultrahigh volume fractions ($0.9 \leq V_V \leq 0.96$) from 2D phase field simulations. We compared our studies with theoretical and experimental studies in grain growth and interface-controlled ripening. We also carefully studied changes of shapes of particles with increase in volume fraction.

Several specific conclusions can be drawn from this study.

(1) Figure 6 shows that the cubic average radius of particles is approximately proportional to time. In other words, under the condition of our simulation, the kinetics of phase coarsening at ultrahigh volume fractions ($0.9 \leq V_V \leq 0.96$) approximately follows the kinetics of diffusion-controlled phase coarsening. This prediction is in good agreement with Sok and Yoon' experimental observation at volume fraction up to $V_V=0.95$ for the system of Co–Cu alloys.[32] However, this prediction is different from the experimental work of Kailasam *et al.*[33] Kailasam *et al.* showed that $\langle R \rangle^3$ is proportional to time at volume fraction up to $V_V=0.95$ for the system of Sn–Pb alloys. To our best knowledge, there exist only two experimental works in which the volume fractions are in the range of $0.9 \leq V_V \leq 0.96$.[32,33]

(2) The PSD's as functions of the dispersoid volume fraction derived from our simulations are shown in Fig. 7. The interesting finding is that the PSD's derived from our simulations at ultrahigh volume fractions are closer to Wagner's PSD rather than Hillert's 2D grain size distribution in grain growth.[44] This suggests that the phase coarsening at ultrahigh volume fractions ($0.9 \leq V_V \leq 0.96$) may be interface-controlled coarsening. At least, the interface-controlled ripening may play more important role than that of diffusion-controlled ripening at ultrahigh volume fractions.

(3) From the snapshots of microstructures in Figs. 2–4, we observed that curved sides of most of particles at volume fraction $V_V \approx 0.90$ gradually change into sharply flattened edges with increase in volume fraction to $V_V \approx 0.96$. Many liquid-filled triple junctions are formed as a result of grain shape accommodation at ultrahigh volume fraction, $V_V \approx 0.96$. This similar phenomenon was also observed in experimental work.[33]

(4) At ultrahigh volume fractions we observed that the peak of the PSD is lowered down and the width of the PSD increases with increase in volume fraction is increased. This is typical characteristics of phase coarsening and also observed at lower volume fractions.

(5) Finally, it is worth noting that there are only two experiments[32,33] at ultrahigh volume fractions. Considering that simulations have made major strides during the past few years, we suggest that new experiments should be designed to derive data that can be quantitatively compared with the rapidly improving predictions derived from simulations. New experimental results will remain fundamentally important to making additional progress in the field of microstructural evolution kinetics. New experimental data are critical to establishing broader, more reliable, quantitative comparisons with theory and simulations.

ACKNOWLEDGMENTS

The authors are pleased to acknowledge partial financial support received from the Materials World Network Program and Metallic Materials and Nanostructures Program of National Science Foundation, Washington, DC, under Grant Nos. DMR-0710484 (Wang) and DMR-0710483 (Chen). The authors (Wang and Ding) are also pleased to acknowledge partial financial support received from Florida Solar Energy Center.

[1] I. M. Lifshitz and V. V. Slyozov, J. Phys. Chem. Solids **19**, 35 (1961).
[2] C. Wagner, Z. Elektrochem. **65**, 581 (1961).
[3] H. V. Atkinson, Acta Metall. **36**, 469 (1988).
[4] V. E. Fradkov and U. Udler, Adv. Phys. **43**, 739 (1994).
[5] K. G. Wang, M. E. Glicksman, and K. Rajan, Comput. Mater. Sci. **34**, 235 (2005).
[6] K. G. Wang and M. E. Glicksman, *Processing Handbook*, edited by J. Groza *et al.* (CRC, Boca Raton, 2007), Chap. 6.
[7] P. W. Voorhees, Annu. Rev. Mater. Sci. **22**, 197 (1992).
[8] A. Baldan, J. Mater. Sci. **37**, 2171 (2002).
[9] A. J. Ardell, Acta Metall. **20**, 61 (1972).
[10] A. D. Brailsford and P. Wynblatt, Acta Metall. **27**, 489 (1979).
[11] C. K. L. Davies, P. Nash, and R. N. Stevens, Acta Mater. **28**, 179 (1980).
[12] K. Tsumuraya and Y. Miyata, Acta Metall. **31**, 437 (1983).
[13] J. A. Marqusee and J. Ross, J. Chem. Phys. **80**, 536 (1984).
[14] J. H. Yao, K. R. Elder, H. Guo, and M. Grant, Phys. Rev. B **47**, 14110 (1993).
[15] M. Tokuyama and Y. Enomoto, Phys. Rev. E **47**, 1156 (1993).
[16] J. Alkemper, V. A. Snyder, N. Akaiwa, and P. W. Voorhees, Phys. Rev. Lett. **82**, 2725 (1999).
[17] S. P. Marsh and M. E. Glicksman, Acta Mater. **44**, 3761 (1996).
[18] J. Weins and J. W. Cahn, in *Sintering and Related Phenomena*, edited by G. C. Kuczynski (Plenum, New York, 1973), pp. 151–163.
[19] P. W. Voorhees and M. E. Glicksman, Acta Metall. **32**, 2013 (1984).
[20] C. W. J. Beenakker, Phys. Rev. A **33**, 4482 (1986).
[21] M. E. Glicksman, K. G. Wang, and S. P. Marsh, J. Cryst. Growth **230**, 318 (2001).
[22] K. G. Wang, M. E. Glicksman, and K. Rajan, Phys. Rev. E **69**, 061507 (2004).
[23] K. G. Wang and M. E. Glicksman, Phys. Rev. E **68**, 051501 (2003).
[24] K. G. Wang, M. E. Glicksman, and C. Lou, Phys. Rev. E **73**, 061502 (2006).
[25] M. E. Glicksman, K. G. Wang, and P. Crawford, *Computational Modeling of Materials, Minerals and Metals Processing*, edited by M. Cross, J. W. Evans, and C. Bailey (The Minerals, Metals & Materials Society, Warrendale, PA, 2001), pp. 703–713.
[26] N. Akaiwa and P. W. Voorhees, Phys. Rev. E **49**, 3860 (1994).
[27] H. Mandyam, M. E. Glicksman, J. Helsing, and S. P. Marsh, Phys. Rev. E **58**, 2119 (1998).
[28] V. E. Fradkov, M. E. Glicksman, and S. P. Marsh, Phys. Rev. E **53**, 3925 (1996).
[29] D. Fan, S. P. Chen, L.-Q. Chen, and P. W. Voorhees, Acta Mater. **50**, 1895 (2002).
[30] A. Baldan, J. Mater. Sci. **37**, 2379 (2002).
[31] S. C. Hardy and P. W. Voorhees, Metall. Trans. A **19A**, 2713 (1988).

[32]S. Sok and D. N. Yoon, Metall. Trans. A **13A**, 1405 (1984).
[33]S. K. Kailasam, M. E. Glicksman, S. S. Mani, and V. E. Fradkov, Metall. Mater. Trans. A **30**, 1541 (1999).
[34]A. Karma, in *Encyclopedia of Materials Science and Technology*, edited by K. H. J. Buschow, R. W. Cahn, M. C. Flemings, B. B. Ilschner, E. J. Kramer, and S. Mahajan (Elsevier, Oxford, 2001), p. 6873.
[35]W. J. Boettinger, J. A. Warren, C. Beckermann, and A. Karma, Annu. Rev. Mater. Res. **32**, 163 (2002).
[36]L. Q. Chen, Annu. Rev. Mater. Res. **32**, 113 (2002).
[37]C. E. Krill III and L.-Q. Chen, Acta Mater. **50**, 3057 (2002).
[38]L. Q. Chen and W. Yang, Phys. Rev. B **50**, 15752 (1994).
[39]A. Kazaryan, Y. Wang, S. A. Dregia, and B. R. Patton, Phys. Rev. B **63**, 184102 (2001).
[40]R. Kobayashi, J. A. Warren, and W. C. Carter, Physica D **140**, 141 (2000).
[41]J. W. Cahn and J. E. Hilliard, J. Chem. Phys. **28**, 258 (1958).
[42]S. M. Allen and J. W. Cahn, Acta Metall. **27**, 1085 (1979).
[43]T. M. Rogers and R. C. Desai, Phys. Rev. B **39**, 11956 (1989).
[44]M. Hillert, Acta Metall. **13**, 227 (1965).